ACS Synthetic Biology

Research Article

pubs.acs.org/synthbio

Wiring Together Synthetic Bacterial Consortia to Create a Biological Integrated Circuit

Nicolas Perry,[†] Edward M. Nelson,[†] and Gregory Timp*

University of Notre Dame, Notre Dame, Indiana 46556, United States

Supporting Information

ABSTRACT: The promise of adapting biology to information processing will not be realized until engineered gene circuits, operating in different cell populations, can be wired together to express a predictable function. Here, elementary biological integrated circuits (BICs), consisting of two sets of transmitter and receiver gene circuit modules with embedded memory placed in separate cell populations, were meticulously assembled using live cell lithography and wired together by the mass transport of quorum-sensing (QS) signal molecules to form two isolated communication links (comlinks). The comlink dynamics were tested by broadcasting "clock" pulses of inducers into the networks and measuring the responses of functionally linked fluorescent reporters, and then modeled through simulations that realistically captured the protein production and molecular transport. These results show that the comlinks were isolated and each mimicked aspects of the synchronous, sequential networks used in digital computing. The observations about the flow conditions, derived from numerical simulations, and the biofilm architectures that foster or silence cell-to-cell communications have implications for everything from decontamination of drinking water to bacterial virulence.

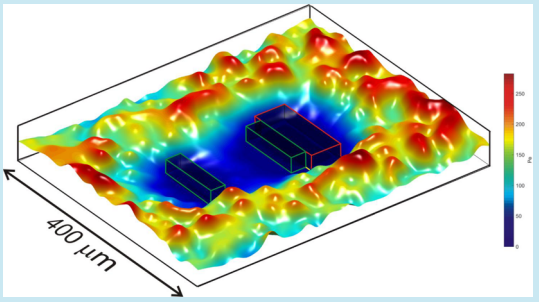

KEYWORDS: *synthetic biology, cell−cell communication, quorum sensing, biological computing, synthetic biofilm*

A living cell perceives and reacts to its environment just like a computer processes information. Accordingly, synthetic biology promises a new paradigm for information processing.[1−5] By rewiring genes, the molecular biology of the cell has already been co-opted to produce all the modules required for a sequential logic network familiar from digital circuit theory: *i.e.*, latches for memory;[6] switches[7] and logic gates (like NOR and NAND)[8−12] have all been synthesized in bacteria. Additionally, it is now possible to synchronize the behavior of gene networks operating in different cells by leveraging cell-to-cell signaling, such as quorum sensing (QS).[13−16] However, with a few exceptions, most of these gene circuits operate within isogenic populations[17−20] to avoid, among other problems, crosstalk between circuits. Moreover, the chemical gradients governing the molecular distributions that mediate cell-to-cell communications are out of control. Thus, the promise of adapting biology to information processing will not be realized until engineered gene circuits, operating in different cell populations, are wired together into a complex consortia—a biological integrated circuit (BIC)—in which control can be exercised over the signaling gradients to coordinate the expression of a predictable computing function.

Bacterial biofilms can inform on suitable topologies for a BIC.[21−23] A native biofilm is dense and consists of a complex heterogeneous community of microbes that reflects many different epigenetic and genetic constituencies, and environmental gradients in nutrients and flow conditions. All this is embedded in an extracellular polymeric substance formed from polysacchrides, proteins and DNA. Within a biofilm, intra-species and interkingdom communications, mediated by small diffusing molecules, occur all at the same time, which can affect the formation, structure and fitness within a particular ecological niche.[23]

In this report, the cell-to-cell communications found in biofilms were mimicked using elementary networks synthesized from two sets of gene circuit modules placed in separate bacteria that transmit or receive two different QS signaling molecules, *i.e.*, acyl-homoserine lactones (HSLs). Generally, in nature, QS involves a transmitter and receiver both in the same cell. The circuitry requires two proteins: (1) an HSL-synthase that produces HSL by leveraging the cell's metabolism; and (2) an HSL-binding protein that acts as a signal receptor and transcriptional activator, respectively.[24,25] In contrast to nature, in this work the QS circuitry was split apart into two independent cell types, a transmitter and receiver, to form a communication link (comlink) that could be distributed spatially.[26] In response to an inducer, the transmitter module coexpressed the HSL-synthase with a fluorescent reporter, whereas the receiver produced the HSL-binding protein along with a fluorescent reporter. Diffusive mass transport of the HSLs and their specificity were then used to wire together bacteria to create well-isolated comlinks. The transmitter produces an HSL that diffuses out of the cell into the microenvironment of the receiver, where it eventually binds to

Received: January 3, 2016

DOI: 10.1021/acssynbio.6b00002
ACS Synth. Biol. XXXX, XXX, XXX−XXX

the activator protein resulting in conformational changes that affect downstream transcription in the receiver.

Independent control was exercised over two comlinks associated with different QS signals: one related to the *lux* system from *Vibrio fischeri*, *N*-(3-oxo-hexanoyl)-L-homoserine lactone ($3OC_6HSL$),[27] and another related to the *las* system from *Pseudomonas auroginosa*, *N*-3-oxo-dodecanoyl-L-homoserine lactone, ($3OC_{12}HSL$).[28] The *Lux* circuits were chosen because many of the parameters that govern the reaction kinetics were already known from other experiments,[14,29−32] making quantitative predictions of the experimental outcomes possible. Moreover, it was known from other work that the *lux*-receiver has embedded memory,[14,29−32] which afforded the opportunity to form an important kind of digital circuit: a synchronous, sequential network. Similarly, many of the parameters governing the *las* circuitry could be estimated from the literature[31,32] due to the apparent homology with *lux*.[24] Interestingly, $3OC_{12}HSL$ mediates, not just intraspecies, but also interspecies and interkingdom communications, which holds out the prospect for multiplexing to other kingdoms,[33,34] although it was not exploited here.

Despite the common moieties (Figure 1a)—both HSLs consist of a homoserine lactone ring that is N-acylated with a fatty acyl group at the α-position—these two signaling molecules potentially offered well-isolated comlinks because each transcriptional activator was supposedly specific to the cognate HSL.[35−38] However, preliminary experiments with the plasmid pFNK-503, which has been proffered as a las-receiver,[20,39] revealed that the receptor protein, lasR, was promiscuous and could be activated with a superfluous concentration of noncognate signal and/or overexpression of the receptor. Actually, this is not unusual since QS networks tend to integrate information gleaned from multiple inputs.[36,40] To suppress the crosstalk, the *las*-receiver genes were re-engineered to enhance specificity.

In addition to multiple comlinks, stringent dynamic control of the chemical gradients and the placement of the cells in them are required to express a predictable, coordinated function. Thus, the components of the two comlinks were assembled into consortia using live cell lithography (LCL).[41] LCL employs multiple, time-shared optical tweezers to form living isogenic voxels by plucking cells from a laminar flow and positioning them on a hydrogel scaffold. To create heterogeneous consortia, arrays of different isogenic voxels were then assembled using a step-and-repeat algorithm.[41] Subsequently, to test the information-carrying capacity of the comlinks, pulses of inducers, such as arabinose and IPTG, were broadcast *via* a microfluidic device into the consortia to produce transient QS signals linked to fluorescent reporters and subsequently the fluorscence was measured. To analyze the signaling dynamics apparent from the fluorescence, deterministic simulations using mass-action kinetics for the protein and signal production were employed, along with finite element simulations (FESs) to account for the advective-diffusive intercellular transport. Thus, the technology files and design rules essential for implementing BICs were developed to model the network performance.

RESULTS AND DISCUSSION

The components of two comlinks were formed by analyzing the *lux* and *las* QS systems into separate sets of transmitter and receiver plasmids, and then transforming *E. coli* (*DH5α*) with them (Figures 1a, S1). The 113 → 203 *lux*-comlink (Figure 1a, top) incorporated transmitter cells that harbored the plasmid

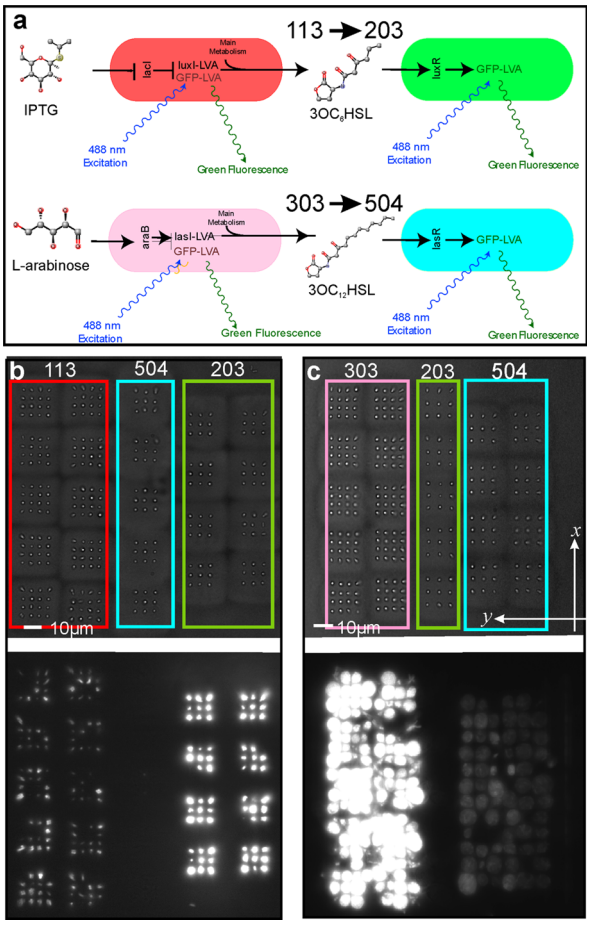

Figure 1. Two independent comlinks were used to form a synthetic bacterial consortia. (a) Schematics representing the 113 → 203 and 303 → 504 comlinks are shown. (top) The 113-transmitter bacteria produced luxI-LVA ($3OC_6HSL$-producing enzyme) as well as GFP-LVA under control of the *lac* promoter induced with IPTG. The 203-receiver bacteria produced luxR ($3OC_6HSL$-binding protein) constitutively under the *luxP(L)* promoter. LuxR binds to $3OC_6$–HSL, then dimerizes and binds to the lux control region, strongly up-regulating *luxP(R)* and weakly up-regulating *luxP(L)*. Upon detection of $3OC_6HSL$, receivers produced GFP-LVA, a rapidly degradable form of GFP. (bottom) The 303-transmitter produced lasI-LVA ($3OC_{12}HSL$-producing enzyme) as well as GFP-LVA under control of the *araB* promoter induced with arabinose. The 504-receiver bacteria produced lasR ($3OC_{12}HSL$-binding protein) constitutively under Lacq promoter. LasR binds to $3OC_{12}HSL$, then dimerizes and binds to the operator in the rsaL gene control region to promote GFP-LVA production. (b) The results of a test of the 113 → 203 comlink are shown. (top) Top-down transmission optical micrograph of a consortium consisting of a 5 × 2 array of 4 × 4 homologous voxels of 113-transmitters (highlighted in red) and a 4 × 2 array of 3 × 3 homologous voxels of 203-*lux*-receivers (highlighted in green) with a 5 × 1 array of 3 × 3 homologous voxels of 504-las-receivers (highlighted in blue) interposed between them. (bottom) A fluorescence image of the same array is shown 6 h after induction with IPTG. (c) The results of a test of the 303 → 504 comlink are shown. (top) Top-down transmission optical micrograph of a consortium consisting of 5 × 2 array of 4 × 4 homologous voxels of 303-transmitters (highlighted in pink) and a 4 × 2 array of 3 × 3 homologous voxels of 504-receivers (highlighted in blue) encapsulated inside a hydrogel with a 5 × 1 array of 3 × 3 homologous voxels of 203 receivers (highlighted in green) interposed between them. (c, bottom) A fluorescent image of the same array is shown 10 h after induction with arabinose.

DOI: 10.1021/acssynbio.6b00002
ACS Synth. Biol. XXXX, XXX, XXX−XXX

113, which had an IPTG-inducible LuxI-LVA (degradable LuxI) gene, coexpressed with a degradable version of the GFP protein (GFP-LVA). The expression of LuxI-LVA in the 113 transmitter facilitated transiently the synthesis of $3OC_6$−HSL by leveraging the cell metabolism until it degraded. The $3OC_6HSL$ diffused across the cell membrane into the environment where it eventually triggered expression in the receiver cells. The *lux*-receivers harbored the 203 plasmid that expressed GFP-LVA when the gene luxR was complexed with $3OC_6HSL$ and bound to the *luxP(L)* promoter. Specifically, the receiver plasmid consisted of the *luxP(L)* promoter controlling luxR production and the *luxP(R)* promoter controlling GFP-LVA production. It has been shown that LuxR, in combination with this promoter, positively autoregulates the QS response by modulating its own expression.[14,30,42] While *luxP(R)* had only a low-level basal expression, it was strongly up-regulated in the presence of the luxR-$3OC_6HSL$ dimer and produced a variant of green fluorescent protein, GFP-LVA, in this case. GFP-LVA was unstable; it degraded by proteolytic digestion with a half-life of about 10−20 min.[43] Thus, gene expression in the *lux*-transmitters and receivers was sensitive to changes in the microenvironment of the cell associated with IPTG and $3OC_6HSL$, respectively.

The 303 → 504 *las*-comlink (Figure 1a, bottom) was formed likewise by analyzing the *las* gene, but it showed a different chemical specificity. The 303-transmitter cells harbored two plasmids: a high copy paraLS plasmid that expressed LasI-LVA under arabinose induction; and a medium copy para203 that also expressed GFP-LVA under arabinose induction. Complementary to the transmitter, the *las*-receiver harbored the 504 plasmid that contained *lasR* downstream of a constitutive promoter and GFP-LVA under a *lasI* promoter so that fluorescent protein was expressed when the receptor protein LasR was activated by exogenous $3OC_{12}HSL$.

The 504 plasmid, designated as pFNK-504I, was similar to the plasmid pFNK-503,[20] except that the *lasR* gene was transcribed from a medium-strength constitutive promoter—the LasR-activated promoter was *LasIp* instead of *rsaLp*—and a transcription terminator was added downstream of the *LasR* gene. Cells transformed with 503 were observed to be sensitive to $3OC_6HSL$, at a threshold of ∼0.5 nM (Figure S2). This observation was consistent with prior work.[36] So, to avoid crosstalk between the two comlinks, the 504 plasmid was constructed, which changed the activation threshold for $3OC_{12}HSL$ from 0.5 nM to 3 nM, while at the same time eliminating the sensitivity to $3OC_6HSL$ for concentrations <1 μM. For 504, the LasIp promoter was chosen to enhance specificity of LasR activation by $3OC_{12}HSL$, because this promoter was shown to be silent when LasR was bound to $3OC_6HSL$, as opposed to other RsaLp.[36] Thus, GFP-LVA expression in the *las*-transmitters and receivers acted as a reporter that was functionally linked to *lasI* and *lasR* gene expression, and sensitive only to changes in the concentration of the arabinose inducer and $3OC_{12}HSL$, respectively.

Preliminary assessments of the chemical specificity of the two comlinks were performed in consortia consisting of isogenic voxels of transmitters and with two different receivers. The test of the 113 → 203 comlink (Figure 1b) was carried out in a consortium that consisted of a 1 × 5 array of 3 × 3 voxels of *las*-receivers (45 cells in all, blue highlight) interposed between a 2 × 5 array of 4 × 4 voxels of 113-*lux*-transmitters (160 cells in total, red highlight) and a 2 × 4 array of 3 × 3 voxels of 203-*lux*-receivers (72 cells, green highlight). The transmission optical micrograph, acquired at t = 0 h just prior to induction with IPTG, revealed that the 203-receivers and 113-transmitter voxels at the top of the image were stitched together into, what amounts to, one hydrogel microstructure with adjacent voxels spaced ∼30 μm apart (in x and/or y). The 504-*las*-receiver array was laid between them, separated from the *lux*-arrays by a microchannel that was about 5 μm-wide and 120 μm-long. (The microchannel was created simply by increasing the spacing between voxels to 35 μm in the y-direction.)

For the test, 700 μM of IPTG in M9 media was broadcast into the microfluidic device containing the network of transmitters and receivers at t = 0 min with a quasi-static flow rate of 0.05 μL/min (3.5 μm/s, on average at the input). Under these conditions, according to FESs, the Péclet number, $Pe < 10^{-7}$, which indicated that the transport was predominately diffusive. The diffusion coefficient of the inducers and HSLs in the hydrogel was estimated to be greater than $D^{\text{hydrogel}}_{\text{rhodamine}} = 17 \pm 10\ \mu m^2/s$, using a fluorescent surrogate with a similar molecular weight.[14] As a result, the inducer concentration was estimated to be practically uniform after broadcasting into the consortium from the microfluidic device, varying <1% throughout within 90 s.[14] After about 1 h, fluorescence was observed above the background in the 113-transmitter array, increasing in intensity continuously after that point so that it could be seen clearly at 2 h, indicating the coexpression of luxI-LVA and $3OC_6HSL$. When the $3OC_6HSL$ concentration in the hydrogel exceeded ∼2 nM[14,30]—near t = 3.7 h—the 203-receivers produced sufficient GFP-LVA to observe fluorescence above the background. (This last assertion followed from FES and controls using exogeneous inducer broadcasts into similar arrays.[14]) The corresponding fluorescence observed in the same consortium at t = 6 h after induction (Figure 1b, bottom) clearly showed that the 113-transmitters were linked to the 203-receivers, whereas no fluorescence was observed in the 504-receivers, indicating that the comlink was well-isolated.

Likewise, a test of the 303 → 504 comlink (Figure 1c) revealed that 303-*las*-transmitters, induced by a 700 μM arabinose broadcast, were linked to 504-*las*-receivers, but not to the 203-*lux*-receivers interposed between them. The onset of fluorescence in the 504-receivers was observed about 10 h after induction, whereas no fluorescence was observed in the 203s, despite the common moieties of the HSLs. Thus, these two signaling molecules, $3OC_6HSL$ and $3OC_{12}HSL$, in combination with these gene circuits, offered well-isolated comlinks suitable intercellular communications without crosstalk.

Parenthetically, one of the main differences between the circuitry in the 203 and 504 plasmids was that the receptor protein in 504 was expressed constitutively, whereas the receptor in 203 was expressed from a promoter that was enhanced when LuxR was activated by $3OC_6HSL$. Thus, the receiver's regulation was in accord with the wild-type QS systems. In *lux* in *V. fischeri*, the autoactivation loop enhances the QS response as more signal becomes available, while the expression level of the LasR receptor in *P. aeroginosa* is constitutive. It also is noteworthy that the *lux* response in *V. fischeri* results in the production of luciferase, whereas the *las* in *P. aeruginosa* is only a part of a more complex gene circuit that is involved in vilurence.[44]

It has been posited that there is not a single cell density for which QS-regulated genes are induced or repressed in intercellular communication systems like these, but rather the signaling is acutely sensitive to mass-transfer.[45] This observa-

DOI: 10.1021/acssynbio.6b00002
ACS Synth. Biol. XXXX, XXX, XXX−XXX

tion is consistent with the view that QS signals act simply as a probe measuring mixing, flow, or diffusion in the microenvironment of the cell.[46,47] To discover the mass transport conditions that elicit a response to a QS signal in these consortia, the effects of hydrodynamic flow combined with transient QS signals induced in the transmitters were tested explicitly (Figures 2−4, S4, S6, S7).

For these tests, another 113 → 203 comlink was formed (Figure 2a) by juxtaposing a 2 × 5 array (of 4 × 4 voxels) of 113s next to two 1 × 4 arrays (of 3 × 3 voxels) of 203s: one immediately adjacent *to* the transmitters (*near*) with a center-to-center separation of 40 μm, and another separated by a gap about 180 μm wide from the transmitters (*remote*). The size of the gap between receivers was stipulated to test the range for communication with a specified number of transmitters. The 113 *lux*-transmitters were driven intermittently ON and OFF using pulses of IPTG to produce $3OC_6HSL$ signal transients in a continuous (transverse) flow of 1.0 μL/min (70 μm/s, on average at the input). Between pulses, the consortium was flushed at 60 μL/min (4.2 mm/s, on average at the input) for 8 min. For a 180 μm wide gap, the delay associated with the signal propagating across the gap was estimated to be insignificant ($\Delta t = L^2/D$ = 1 min), whereas the gradient was expected to be substantial based on FES (Figure 2f).

Starting at time t = 0, 700 μM of IPTG was broadcast into the consortium at a 1.0 μL/min flow rate to induce the production of $3OC_6HSL$ in the 113s, and the resulting intensity of the fluorescence of each region of interest (ROI) was captured and tracked over time (Figure 2b−d, left). The 1.0 μL/min flow rate corresponds to quasi-static conditions since the peak fluid velocity was only about 80 nm/s in this microfluidic in the plane of the biofilm according to FES (Figure 2e). After about 3 h, weak fluorescence was observed in the transmitter array (Figure 2b), indicating the production of $3OC_6HSL$ that, in turn, diffused out of the cells and into the environment. Once fluorescence was observed in the transmitters, the IPTG broadcast was terminated (near t = 5 h), but the flow rate of M9 medium was maintained at 1.0 μL/min until t = 8.3 h, at which time IPTG was again broadcast into the consortium at 700 μM concentration for 1.7 h at 1.0 μL/min. During this interval, for the first time, fluorescence was observed in the *near*-receiver array about 10 min after the onset of the IPTG broadcast (Figure 2c), whereas no response was observed from the *remote*-array (Figure 2d). The consortium was exposed to another IPTG broadcast and flush cycle, starting at 12.5 h. Finally, after the third broadcast of IPTG, fluorescence was observed, not only in the *near*-203 array, but also in the *remote*-203-array after a 30 min delay from the onset of the IPTG broadcast to the 113s. Interestingly, the gradient, in combination with the GFP-LVA production rate, apparently combined to introduce a delay in the response to a signal broadcast.

To elucidate the origin of the delays between the fluorescence in the 113-transmitter and *remote*- and *near*-203 receiver arrays, protein and signal production were simulated deterministically and the mass transport was calculated with FES. These simulations were actually fit to the data using the models represented in Figure S3a to solve the set of eqs S(i−xxiv) offered in the supplement, constrained by the parameters specified in Tables S1−S3 (see Methods). The simulations of the 113 → 203 comlink were performed using conditions that corresponded precisely with experimental conditions and

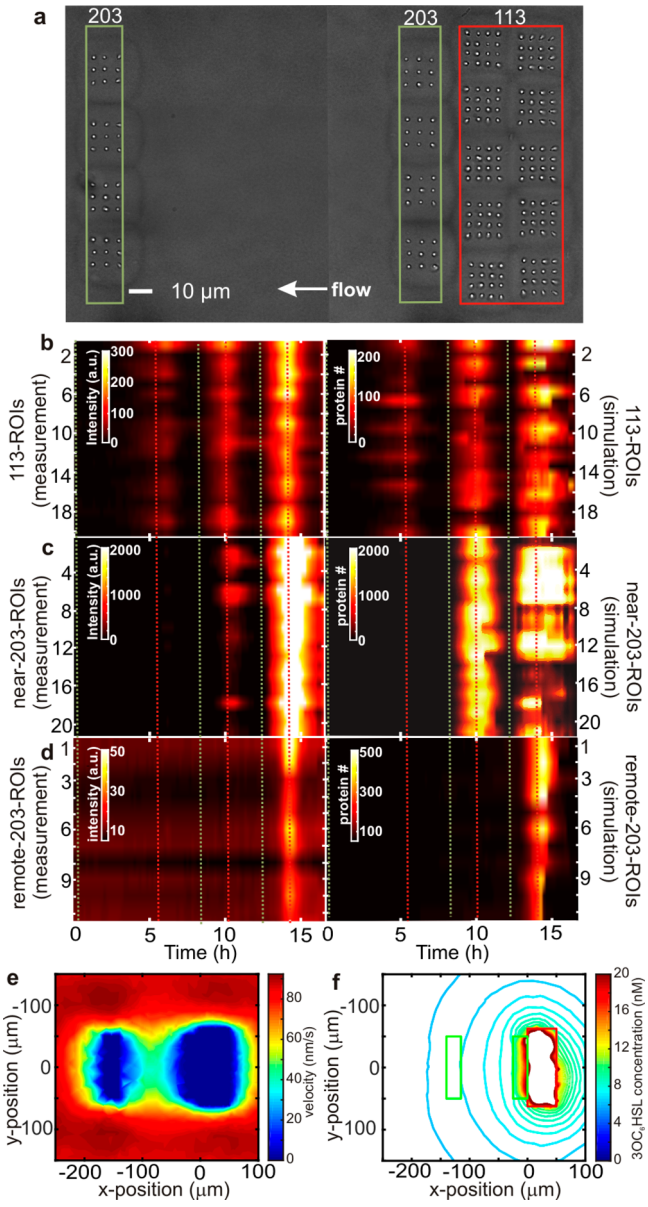

Figure 2. Signaling dynamics in a comlink formed from arrays of 113-*lux*-transmitters and 203-*lux*-receivers. (a) An optical transmission image (t = 0 h) of a consortium, consisting of a 5 × 2 array of 4 × 4 voxels of 113-transmitters (highlighted in red) upstream from two 4 × 1 arrays of 3 × 3 voxels of 203-receivers (highlighted in green), is shown. The transmitter array was separated from the *near*-receiver array by a channel about 5 μm wide and 120 μm long oriented perpendicular to the flow, whereas the *remote*-receiver array was separated from the transmitters by a channel about 180 μm wide and 120 μm long. The arrow indicates the flow direction. (b−d, left) Kymographs showing the fluorescence intensity as a function of time, corresponding to individual ROIs comprising the consortium in (a), are shown. The introduction of the IPTG inducer commenced at the times indicated by the green dotted lines and sequentially terminated at the red lines. Signaling was initiated at t = 0 by broadcasting 700 μM IPTG into the microfluidic under quasi-static flow conditions (1.0 μL/min), which induced $3OC_6HSL$ production in the 113 transmitters. At t = 2.5 h, weak fluorescence was first observed in the transmitter array. At t = 5 h, IPTG broadcast was terminated and the arrays were flushed with medium at a flow rate of 60 μL/min (4.2 mm/s) for 0.13 h (8 min), and subsequently the system was allowed to recover in a quasi-static flow. Similarly, the system was induced with IPTG at 7.5 h and flushed again at t = 9 h and induced once more at 11.2 h and flushed

DOI: 10.1021/acssynbio.6b00002
ACS Synth. Biol. XXXX, XXX, XXX−XXX

Figure 2. continued

again at 13 h and allowed to recover. Weak fluorescence was first observed in the *near*-receiver array at about t = 8 h. (b–d, right) The corresponding kymographs of the fluorescent protein number, acquired from deterministic simulations performed under similar conditions to the experiment, are shown, which reveal the same behavior as a function of the flow conditions and time. (e) An FES of the fluid velocity in the microfluidic in the plane of the consortium is shown. (f) A contour plot of the simulated $3OC_6HSL$ concentration superimposed over a schematic represention of the consortium is shown.

reported the number of fluorescent molecules produced (Figure 2b–d, right).

Remarkably, the simulations accounted for all the experimental outcomes, including the transmitter and *near*- and *remote*-receiver fluorescence patterns, even though the parameters were tightly constrained. Therefore, an accurate assessment of the signal gradients and mass transport could be inferred from them with FES. The simulations revealed that the quasi-static flow conditions and the proximity, along with the hydrogel scaffold, ensured mimimal advective transport within the consortium, *i.e.*, $Pe < 10^{-7}$ in the hydrogel between the *near*-receiver and transmitter arrays, and $Pe < 10^{-4}$ in the hydrogel between the *near*- and *remote*-receiver arrays, so that the transport was predominately diffusive there, whereas outside the consortium $Pe > 10^{-3}$ (Figure S4).[29] A comparison of the resulting signal concentration gradients during the first IPTG pulse (Figure 2f) revealed a sharp gradient in the signal produced by the 113s, which nevertheless did not exceed the threshold for detection in either the *near*- or *remote*-receiver arrays. However, during the second pulse, although the gradient was still just as sharp, the signal level from the 113-transmitters increased so that the $3OC_6HSL$ threshold was exceeded in the *near*-array. The simulation puts the $3OC_6HSL$ concentration at 5 nM in the *near*-array, resulting in the production of more than 500 LuxR molecules per cell by t = 6.5 h, whereas the concentration was only 0.5 nM in the *remote*-array, which corresponded to <1 molecule of $3OC_6HSL$ in the cell volume—well below the bifurcation threshold—with no additional LuxR produced above that expressed constitutively.

For the 203 receiver circuit in the 113 → 203 comlink, it was previously reported that memory was invested in the amount of LuxR in each cell that, in turn, affected the sensitivity of the bacteria to $3OC_6HSL$ exposure.[14,30,42] In particular, it has been shown using laser cytometry that induction of these 203-receivers was hysteretic and bistable,[14,30] in correspondence with the up-regulation of luxR with inducer as demonstrated using RT-PCR.[30] High levels of LuxR (HIGH state) allow the bacteria to respond to lower levels of the HSL, whereas cells with low levels of LuxR (LOW state) were unresponsive without higher levels of HSL. Changes in the memory status can occur either through production of LuxR *via* induction with HSL (LOW → HIGH), or *via* dilution of the LuxR concentration over time through cell division (HIGH → LOW).[14] Thus, combined with the memory of the first pulse, the *near*-array fluoresced when the HSL concentration exceeded the bifurcation threshold during the second IPTG pulse. On the other hand, during the third broadcast of IPTG, the 113 transmitters produced a signal strength that exceeded the $3OC_6HSL$ induction threshold in both the *near*- and *remote*-receiver arrays, and the memory of the first and second pulses, combined with this flux on the *remote*-array resulted in fluorescence. Thus, the delay in the fluorescence between the *near* and *remote*-receiver arrays was inextricably linked to the concentration of LuxR in the individual receiver elements, which depended on the current input and the history of inputs.

Similarly, judging from the delays, the activity observed in the 303 → 504 comlink evinced a memory component too, ostensibly related to the lack of a freely diffusible signal. The 303 → 504 comlink consisted of a consortium (Figure 3a) formed from a 2 × 4-array (of 3 × 3 voxels) of 504s (72 *las*-receivers in total) adjacent to a 2 × 5-array (of (4 × 4) voxels) of 303-*las*-transmitters (160 in total). To force gene expression, the 303-transmitters were repeatedly induced using 700 μM pulses of arabinose in a constant flow of 1.0 μL/min to produce $3OC_{12}HSL$. Two hours after assembly, arabinose was broadcast into the consortium for 3 h and then flushed with medium (M9) at the same flow rate (1.0 μL/min) until t = 7 h, at which time arabinose was broadcast into it again for another 2 h. The ROIs revealed fluorescence in the 303-transmitter array at about t = 3.5 h, indicating the production of $3OC_{12}HSL$ (Figure 3b, left). Presumably then, $3OC_{12}HSL$ was diffusing out of the transmitters and into the extracellular environment, but no response was observed in the 504-receivers driven by 303s until after t = 9 h, just after the termination of the second arabinose induction pulse starting at t = 7 h. The 504-receiver fluorescence peaked just before t = 12 h, while the consortium was still being flushed. However, the fluorescence decay rate in both the transmitter and receiver were similar—it generally took about 2 h for the fluorescence to return to the baseline.

These data were augmented by calibrations performed by broadcasting exogeneously $3OC_{12}HSL$ into *las*-receiver arrays. (Figure S5 is an example acquired for a near-threshold HSL concentration of 3 nM). The calibrations revealed several interesting features: (1) even near-threshold (~3 nM $3OC_{12}HSL$), the fluorescence in the array could be observed within about 1 h after a broadcast of HSL; (2) the response time, defined as the time to reach halfway between the initial and final levels, was $\tau_{50\%} \sim 1$ h; (3) the fluorescence persisted without attentuation long after the inducer/HSL was flushed; and (4) finally, the response to HSL broadcasted exogenously into 504 *las*-receiver arrays, consisting of differently sized voxels, was observed at practically the same time (within about 10 min) regardless of the size, which indicated that the delays observed in the *las*-comlink should not be attributed to slow diffusion in the hydrogel. Taken together, these data were inconsistent with the assertion that an HSL with a longer side-chain length has a higher binding affinity to its cognate LuxR-type regulator,[48] since the GFP-LVA production/decay rate, inferred from the fluorescence in both the *las*-transmitter and receiver, was practically the same as observed in the *lux*-transmitter and receiver ($\tau_{50\%} \sim 1$ h). These data also indicated that LasR binds reversibly to the promoter, contrary to other work.[37]

The delay between the onset of fluorescence in the 504 *las*-receiver and the 303 transmissions and the duration of the receiver response could be interpreted as evidence of a weak (*lasI*) promoter, but it is unlikely. Some promoters responded to the addition of HSL early in culture growth, and others showed a substantial delay, responding to signals only in the stationary phase. However, *araBp* and *lasIp* are both considered strong promoters in the logarithmic growth phase from which the 303 and 504 bacteria were taken (Methods). Instead, to account for the dynamics, it was hypothesized that the

DOI: 10.1021/acssynbio.6b00002
ACS Synth. Biol. XXXX, XXX, XXX–XXX

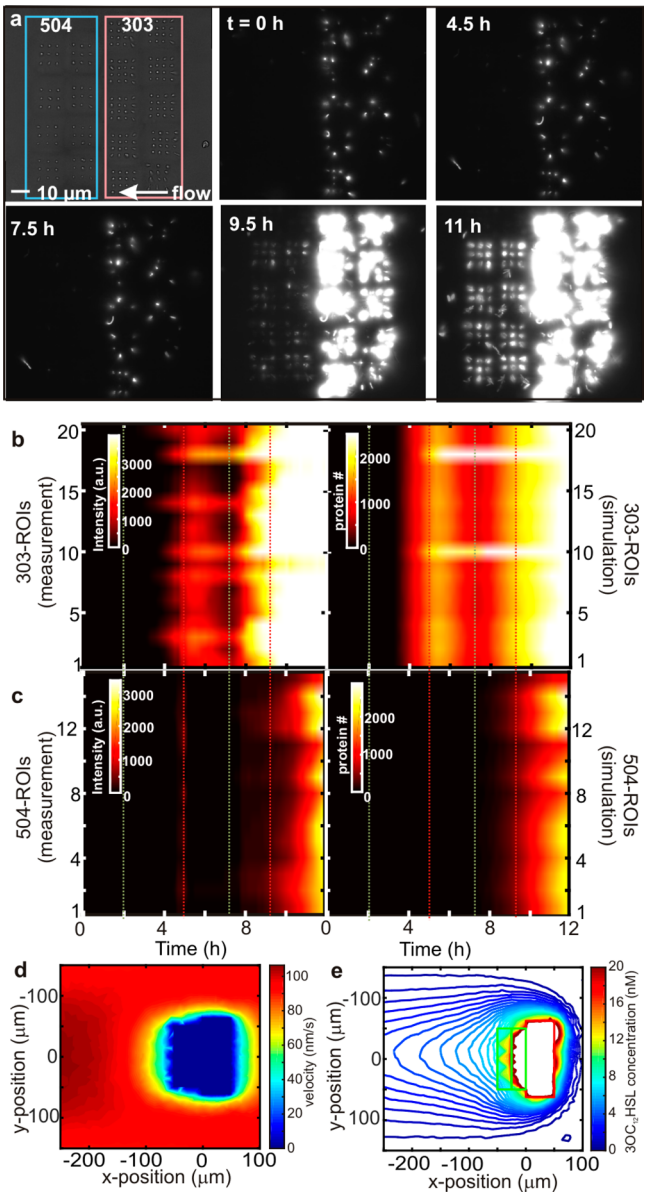

Figure 3. Signaling dynamics in a comlink formed from arrays of 303-las-transmitters and 504-las-receivers. (a) An optical transmission image (t = 0 h) and fluorescence images taken at t = 0, 4.5, 7.5, 9.5, and 11 h are shown of a consortium consisting of a 5 × 2 array (of 4 × 4 voxels of) 303-transmitters (highlighted in pink) upstream of a 4 × 2 array (of 3 × 3 voxels of) 504-receivers (highlighted in blue). The array of transmitters was separated from the receiver arrays by a channel about 5 μm wide and 100 μm long oriented perpendicular to the flow. The arrow indicates the flow direction. (b–c, left) Kymographs of the fluorescence intensity as a function of time are shown, corresponding to individual ROIs comprising the consortium in (a). The introduction of the arabinose commences at the times indicated by the green dotted lines and terminates at the red lines. Signaling was initiated at t = 2 h by broadcasting 700 μM arabinose into the microfluidic under quasi-static flow conditions (1.0 μL/min), which induces $3OC_{12}HSL$ production in the 303-transmitters. After about 1 h (at t = 3.2 h), weak fluorescence was observed in the transmitter array. At 5 h the arabinose broadcast was terminated and the arrays were flushed at a flow rate 10 μL/min for 0.7 h with medium, and subsequently the system was allowed to recover in quasi-static flow. Similarly, arabinose was again broadcast at 7.2 h and flushed at 9.2 h for 0.7 h with medium. (b–c, right) The corresponding kymographs of the fluorescent protein number, acquired from simulations performed under similar conditions to the experiment, are shown that reveal the same behavior as a function of the flow conditions and time. (d) An FES of the fluid velocity in the microfluidic in the plane of the consortium is shown. (e) A contour plot of the simulated $3OC_{12}HSL$ concentration, superimposed over a schematic represention of the consoritium, is shown.

fluorescent response of the 504-receivers reflected, not only the production of lasI, HSL and lasR, but also a limitation in the transport of the $3OC_{12}HSL$ signals across the *E. coli* membrane. Although it has been shown that $3OC_{12}HSL$ can permeate the *E. coli* membrane and remain functional,[37] it does not diffuse freely across the *P. aeruginosa* membrane since the steady-state intracellular concentration is 3-fold higher than the extracellular concentration.[49] Moreover, when a known efflux system was inhibited, the concentration of intracellular $3OC_{12}HSL$ was higher than observed in wild-type cells, which suggests active efflux of $3OC_{12}HSL$ across a relatively impermeable membrane.[49] Finally, the transport of long-chain HSLs in *Sinorhizobium meliloti* was facilitated by *FadL*,[50] which is homologous to *FadL* in *E. coli* with a similar function. Taken altogether, the literature supports the notion that, unlike $3OC_6HSL$, $3OC_{12}HSL$ does not freely diffuse across the cell membrane in gram-negative bacteria, including *E. coli*. Thus, it was postulated that the slow response of the 504-receivers was attributable to partitioning or sequestration of the $3OC_{12}HSL$ signal in the *E. coli* membrane.

On the basis of this reasoning, numerical simulations of the *las*-comlink were used to validate the various contributions to the signal dynamics. A model was constructed (Figure S3b) to describe the 303 → 504 comlink, which was similar to the one used for the 113 → 203 comlink, except that two additional compartments surrounding the 303-transmitter and 504-receiver, were added along with transport coefficients that describe the influx and efflux of $3OC_{12}HSL$ between the extracellular space and the membrane, and between the membrane and the intracellular space. In particular, in terms of the deterministic model offered in the supplement, the sequestration is treated as diffusion with two different rates. The rate equation that describes the transfer of $3OC_{12}HSL$ (A) into and out of the membrane (A_{mem}) is given by the following equation:

$$\frac{d[A_{mem}]}{dt} = D_1([A] - [A_{mem}]) - D_0([A_{mem}] - [A_{ex}])$$

A delay in the accumulation of the intracellular and extracellular concentrations of $3OC_{12}HSL$ (A, A_{ex} respectively) develops from differences in D_1 (diffusivity of $3OC_{12}HSL$ into the cell) and D_0 (diffusivity of $3OC_{12}HSL$ into the membrane). Thus, diffusion into and out of these compartments was used to account for the partitioning and/or sequestration of $3OC_{12}HSL$ in the cell membrane (eqs S(xxv–li) and Tables S4–S6). Similar to the *lux*-comlink, the quasi-static flow conditions (1.0 μL/min), the hydrogel scaffold and close proximity, ensured that diffusive transport predominated, *i.e.*, $Pe < 10^{-7}$ within the consortium (Figure S6)—and so, concentration gradients developed between the *las*-receivers and transmitters (Figure 3d,e).

Comparing the kymographs derived from deterministic simulations (Figure 3b,c, right) with the corresponding empirical data (Figure 3b,c, left), it was apparent from the results of numerical simulation that it was possible to account

DOI: 10.1021/acssynbio.6b00002
ACS Synth. Biol. XXXX, XXX, XXX–XXX

for the delays observed in the fluorescence with the parameters of Tables S4−S6, although these choices were not unique. According to this interpretation of the data, the delays were associated with diffusion of $3OC_{12}HSL$ into and out of the cell membranes. Depending on the history of the inputs, the membranes acted like a source or a sink for the HSL. The delay in the onset of the fluorescence in the 504 *las*-receiver was then related to both the available number of intracellular HSL molecules affected by the membrane as well as the production of LasR. Thus, like 113 → 203, the 303 → 504 comlink also had memory, which was invested in the amount of $3OC_{12}HSL$ in the transmitter and receiver cytosol and sequestered in their respective membranes, as well as the number of LasR molecules in the receiver. This memory was likened to the dynamic random-access memory (DRAM) used in electronic digital computing, which stores information in a separate capacitor within an integrated circuit that can either be charged or discharged. The charge on the capacitor represents two values of a bit, but it is transient because even an OFF-transistor leaks and so the capacitor must be refreshed regularly.

Finally, relying on the specificity of each receptor protein for its cognate signal to check the crosstalk, a 303 → 504 comlink was juxtaposed in the same consortium with 113 → 203 *lux* (Figure 4a) and the two were tested sequentially. The consortium was formed using a 113 → 203 *lux*-comlink consisting of a 5 × 1-array (of 4 × 4 voxels) of 113s (80 total) adjacent to a 4 × 1-array (of 3 × 3 voxels) of 203s (36 total) separated by only 26 μm center-to-center. Immediately adjacent to the *lux*-comlink was a 2 × 4-array (of 3 × 3 voxels) of 504s (72) adjacent to a 5 × 1-array (of 4 × 4 voxels) of 303 *las*-transmitters (80 total). Subsequently, the *las* and *lux*-arrays comprising the two comlinks were induced repeatedly and sequentially with the two inducers, arabinose and IPTG, in a constant flow of 1.0 μL/min. Starting at time t = 3 h, 700 μM of arabinose was broadcast into the array for 2 h to induce the *arab*-switch to produce $3OC_{12}HSL$ in the 303s. After that, the flow rate (of M9) was maintained at 1 μL/min until t = 7 h, at which time 700 μM of IPTG was broadcast for 2 h to induce the 113-transmitters to produce $3OC_6HSL$. This cycle was repeated, beginning at t = 11 h and again at 15 and 19 h.

Kymographs tracking the fluorescence of each ROI in the 303 → 504 (Figure 4b,c, left) and 113 → 203 comlinks (Figure 4d,e, left), respectively, revealed the dynamics of gene expression. Following the start of the second broadcast of arabinose at t = 11 h, fluorescence was observed in the 303-transmitter array indicating the production of $3OC_{12}HSL$ that eventually diffused out of the cells and into the environment. Although the arabinose broadcast was terminated at t = 13 h, the onset of fluorescence was observed in the 504-receiver array just after t = 14 h, after about a 2 h delay from the onset of fluorescence in the transmitters. When the second arabinose broadcast was terminated, a second IPTG broadcast commenced at t = 15 h, which continued for 2 h. Fluorescence was finally observed in the 113-transmitter array near t = 16.2 h, and then in the adjacent 203-receiver array less than 30 min later. On the basis of these observations, it appears that the *lux*- and *las*-comlinks were well isolated—the *lux*-circuitry did not respond to the 303-*las*-transmitters, nor did the *las*-circuitry show a response to the 113-*lux*-transmitters. Moreover, the kymographs of the simulated responses, accomplished using the parameters delineated in Tables S1−S6 and eqs S(i−li), which corresponded precisely to the experimental conditions, evidently captured the main features of the experiment, *i.e.*,

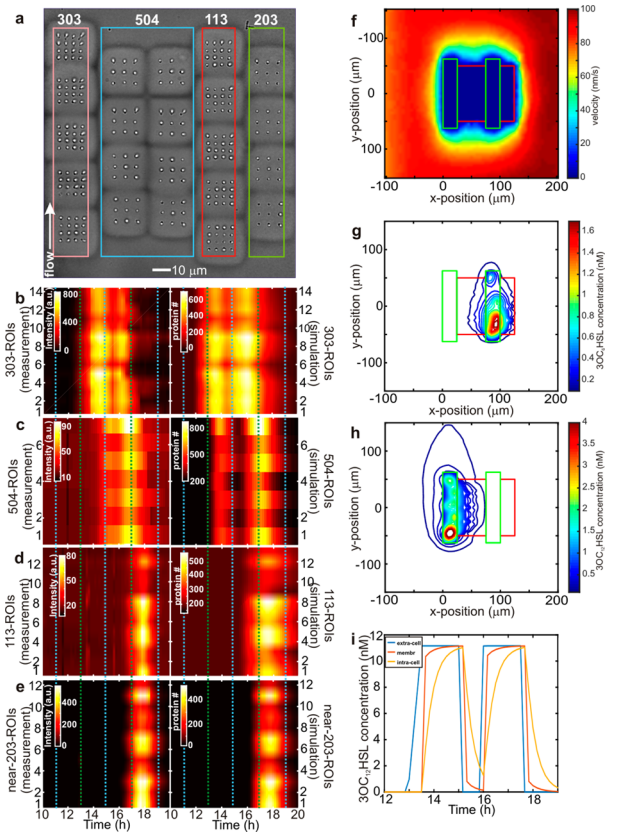

Figure 4. Signaling dynamics in consortium consisting of two comlinks formed from arrays of 113 → 203 and 303 → 504, respectively. (a) An optical transmission image is shown, which was acquired at (t = 0 h) from a consortium consisting of a 1 × 5 array of 4 × 4 voxels of 113-transmitters (highlighted in red) adjacent to a 4 × 1 array of 3 × 3 voxels of 203-receivers (highlighted in green), juxtaposed with an array 5 × 1 array of 4 × 4 voxels of 303-transmitters (highlighted in pink) adjacent to a 4 × 2 array of 3 × 3 voxels of 504-receivers (highlighted in blue). The arrow indicates the flow direction. (b−e, left) Kymographs depicting the fluorescence intensity as a function of time are shown, which correspond to individual ROIs comprising the consortium in (a). Arabinose was repeatedly broadcasted into the consortium at the times indicated by the blue dotted lines, terminating on the green dotted lines. On the other hand, IPTG was repeatedly broadcasted into the consortum starting at the times indicated by the green dotted lines, terminated on the blue dotted lines. Signaling was initiated at t = 3 h by broadcasting 700 μM arabinose into the microfluidic under quasi-static flow conditions (1.0 μL/min) to induce $3OC_{12}HSL$ production in the 303-transmitters. After 2 h, the arabinose broadcast terminated and a 2 h 700 μM broadcast of IPTG commenced immediately and the cycle repeated. After the second cycle of arabinose, fluorescence was observed in the 504, but not the 203-receivers. The 113-transmitters only fluoresced after 16 h at which time the 203-receivers fluoresced. (b−e, right) The corresponding kymographs of the fluorescent protein number acquired from simulations under similar conditions to the experiment are shown, which reveal the same behavior observed empirically as a function of the flow conditions and time. (f) An FES of the fluid velocity in the microfluidic in the plane of the consortium is shown. (g,h) Contour plots of the simulated $3OC_6HSL$ and $3OC_{12}HSL$ concentrations are shown, respectively, superimposed over schematic representions of the consoritium. (i) The line-plot shows extra-cellular (blue line), intracellular (yellow line) and membrane (red) concentration of $3OC_{12}HSL$ associated with a 504 *las*-receiver derived from the same simulations, which illustrate the embedded memory.

DOI: 10.1021/acssynbio.6b00002
ACS Synth. Biol. XXXX, XXX, XXX−XXX

the onset, rise and fall times of the fluorescent response as well as the delays (Figure 4b−e, right).

Under these conditions, FESs indicated that the transport in the consortium was diffusive with $Pe < 10^{-7}$ (Figures 4f, S7) and so concentration gradients developed between the receivers and transmitters (Figure 4g,h). Since they were immediately adjacent, the memory embedded with luxR in the *lux*-receiver produced a response that was nearly synchronous with the 113-transmitters. In contrast, however, the effect of the memory in the *las*-comlink was clearly observed in the delay and persistence of the *las*-receiver fluorescence. The simulations captured the delay and persistence through sequestration of $3OC_{12}HSL$ in the membrane (Figure 4i).

Thus, elementary gene circuits were synthesized that acted like transmitters and receivers for two naturally occurring QS signals, $3OC_6HSL$ and $3OC_{12}HSL$, bacteria were transformed with them, and then the bacteria were assembled into consortia wired together by the mass transport of QS signals. The gene circuitry was engineered to be highly specific to the cognate transcriptional activator so as to provide well-isolated communication channels that enabled multiple biochemical inputs and parallel interconnections between the bacteria. The construction of these synthetic consortia, along with the tools used to analyze the dynamics of the signaling in the comlinks, provides a framework for exploring how naturally existing cellular components can be assembled to program and coordinate complex cellular behavior.

Analyzing the properties of bacterial signaling networks can illuminate the principles underpinning their organization and ultimately offer a guide to strategies for network synthesis. One salient feature of these networks is crosstalk.[51] QS networks can integrate information gleaned from multiple inputs. For example, due to crosstalk, the *lux*-genes in *V. fischeri* do not seem to discriminate between $3OC_6HSL$ and C_8HSL so that *lux* regulation can become noisy,[40] which could be used to suppress or even enhance the sensitivity of a gene switch.[14,39]

What is new in this report is that information (associated with the pulses of inducers, IPTG and arabinose) was transmitted in isolated channels by diffusion of QS signal molecules to receivers with embedded memory, and coordinated through the precise placement of the transmitting and receiving elements and inducer clock pulses to create predictable responses. Diffusive, dispersive signal transmission like this also occurs in dendritic processes in neurons, which form the basis for information processing in the nervous system.[52] Dendrites are the thread-like extensions of the cytoplasm of a neuron that act like wires conveying information over short distances. Whereas the electrical resistance associated with a dendrite isolates the computations between different synapses in the same dendritic tree, the isolation between comlinks in this work was achieved because each transcriptional activator was specific to the cognate HSL. Digital computing relies on isolated information channels like this to connect logic gates.[53] For combinatorial logic used for digital computing, the output is purely a function of well-defined inputs. However, a sequential network merges combinatorial logic with information storage devices, *i.e.*, memory. Such a network receives an input and produces an output that is a function of both the current input and the history of the inputs. Although no combinatorial logic was performed here, both the *lux*- and *las*-comlinks incorporated memory elements, qualifying them as elementary sequential networks.

A sequential network is defined by three sets of equations called the *output* equations, the *next-state* equations, and the *register control* equations. The deterministic simulation tools developed here captured the essential aspects of these equations by analyzing the spatial and temporal development of fluorescent protein production in a consortium. The modeling of the networks described in Figures 2−4, within narrowly defined parameters, demonstrated that it was possible to infer information about protein production and attrition required to determine accurately the dynamics of the consortia. Finally, a synchronous, sequential network uses a clock to synchronize the operation of the parts of the network. Ideally, the stored information changes only during a clock pulse. Between pulses, logical operations are performed on the input and stored information, but there is no change in the stored information. Both the *lux*- and *las*-comlinks were clocked exogeneously by pulses of the arabinose and IPTG chemical inducers. With the introduction of logic gates, the interval between inducer pulses would have to be long enough to accommodate logical operations, but short enough to avoid the need to refresh the transient memory in the comlinks.

The analysis of these circuits has revealed several shortcomings for applications in digital computing. Even with these simulation tools, designing synchronous, sequential networks is hard to do. Although the synchronous design process is generally heuristic, it can nevertheless be analyzed into the following steps according to Booth:[53] (1) description of the operating specifications, which identifies all inputs and outputs and the relationship between them; (2) determination of a state table derived from the specifications established in step 1; (3) optimization of the state-table, which satisfies the operational requirements without introducing redundant or unnecessary states; (4) encoding the information into binary form that transforms the state table into a transition table that describes the properties of the next state and the output functions; and finally, (5) accounting for the operational characteristics of the storage element, the logical operations connecting the input and present state to the output and control signals can be derived. The technology files (Tables S1−S6) and design rules essential for the design and the implementation of BICs have been developed in this work to model the performance and facilitate this type of network design, but the simulations were time-consuming (hours). Figures 2−4 also illuminate two other shortcomings for biocomputing: the slow speed ($\tau_{50\%} \sim 1$ h) that is limited mainly by protein/signal production or attrition rates; and the signal attentuation by diffusion over distances >100 μm. The slow speed can be attended by cell proliferation during a computation cycle (which could adversely affect memory), but this might be compensated by using a single-protein production strategy that forces a cell into a quasi-quiescent state without affecting targeted protein production.[14,54] Also offsetting the slow speed is the possibility for parallel computation available through multiple, practically identical voxels created by LCL with a step-and-repeat algorithm. Arrays of any size and shape can be constructed this way. Moreover, as demonstrated elsewhere, even three-dimensional circuitry is possible by stacking voxels so that fan-out could be increased.[55] Alternatively, the logic could be made to switch faster.[56] Finally, embedded memory, and the bistability that drives it, could be used to mitigate signal attentuation.[39]

Although these BICs represent only a modest first step, elaborations on the synthetic consortia created here could also

DOI: 10.1021/acssynbio.6b00002
ACS Synth. Biol. XXXX, XXX, XXX−XXX

serve as models for rigorously testing hypotheses regarding phenotype diversity in a biofilm since both cell-to-cell communications and the cytoarchitecture can be manipulated at the same time. For example, the observations about the flow conditions and the network architectures that foster or silence cell-to-cell communications among the constituents in a biofilm have implications for everything from the hydraulic conditions required for decontamination of drinking water distribution systems[57] to persistence in tuberculosis granulomas and metastatic (cancer) niches. In particular, in a water distribution system, the complexity of the biofilms can be affected by environmental conditions such as the fluidic shearing force, which can influence the population dynamics.[58] The distribution of phenotypes in a biofilm can confer a survival advantage for opportunistic pathogens over planktonic cells, *e.g.*, higher resistance to antimicrobial agents.[59,60] Thus, these synthetic consortia could be used to study the fate and persistence of pathogens in a biofilm, by varying the cytoarchitecture, the flow conditions, or the concentration of antimicrobials.

METHODS

Genetically Engineered Bacteria. *E. coli* (*DH5α*) was transformed with the *lux*-transmitter plasmid p113 (4.5 Kbp) and the receiver plasmid 203 (3739 bp). The Las transmitter cells consisted of *E. coli* cotransformed with paraLS and para203 (303). Las receiver cells were transformed with plasmid 504 (Figure S1). The transformed bacteria were grown in M9 (0.2% glycerol) minimal media supplemented with 200 μM thiamine and 0.2% (w/v) casamino acids with either ampicillin (100 μg/mL) or kanamycin (100 μg/mL) as a selection marker. They were grown overnight at 37 °C, diluted 1:20 into fresh media, regrown at room temperature, and harvested when they reached an optical density (OD_{633}) of 0.6−0.7. The bacteria were then centrifuged twice at 2.8 rcf for 2 min. Between each spin cycle the supernatant was aspirated, and the bacterial pellet resuspended in M9 media. After the final wash the bacteria were resuspended in M9 (0.2% glycerol) containing the photoinitiator, 2-hydroxy-2-methyl-propiophenone, at a concentration of 0.2% (v/v). Subsequently, the cell suspensions were loaded into individual 1 mL syringes and injected into microfluidic devices through PTFE tubing.

Microfluidic Device. As described elsewhere,[14] laminar fluid flows in a microfluidic device were used to convey cells to an assembly area. The microfluidic was formed from poly dimethylsiloxane (PDMS, Sylgard 184, Dow Corning) using a mold-casting technique. The Sylgard was mixed thoroughly at a 10:1 ratio of epoxy to curing agent. The mixture was then degassed at house vacuum for 60 min and poured into the mold, degassed again for another 60 min. And then cured at 75 °C for 4−6 h. After cooling, the PDMS was peeled away from the mold. The resulting device was 150 μm tall, 1 mm wide and 1 cm long and consisted of three entry-channels, each 200 μm wide that merged together at an angle of 15° and then separated again into three channels, each 250 μm wide and 150 μm tall. The middle channel was used to assemble the BIC.

The transparent microfluidic chip was bonded to #1 cover glass to gain optical access through the bottom of the chip. To seal the microfluidic to the cover glass, an oxygen plasma (Harrick PDS-001, 25 W, 3 min. 20% O_2) was used to produce silanol (Si−OH) groups on the surface of PDMS and on glass. The microfluidic device was gripped by the sides and placed in contact with the cover glass. A uniform pressure was applied to the cover glass for 10 s and subsequently the devices were baked at 75 °C for 2 h to react the silanol groups on the glass surface and PDMS to form a strong covalent siloxane (Si−O−Si) bond. To avoid bacterial adhesion and for greater hydrogel adhesion, the internal surface of the microfluidic was treated with methacrylate silane immediately after bonding the PDMS to the glass coverslip. A 2% (v/v) solution of 3-trimethoxysilylpropyl methacrylate was made in 10.0 mL of 95% ethanol. The solution was adjusted to a pH of 5.0 using 50.0 mL of glacial acetic acid. A milliliter of this solution was pushed through the microfluidic chip and incubated at room temperature for 5 min. Then the excess unreacted methacrylate solution was flushed out with 5.0 mL of deionized water and the chip was baked in an oven overnight at 75 °C. Finally, the microfluidic channel was connected to external fluid reservoirs/syringe pumps through a hole punched in the silicone chip at the input and output ports using a blunt syringe needle.

Live Cell Lithography (LCL). The microfluidic channel was used to convey genetically engineered bacteria to the assembly area where they were organized into living voxels on a hydrogel scaffold using optical tweezers without loss of viability as previously described.[14] Briefly, the optical tweezers were formed at λ = 900 nm using a tunable CW Ti:sapphire laser (Spectra Physics) pumped at 532 nm by a 10 W Nd:YVO_4 diode-pumped solid state laser (Spectra Physics). Acousto-optic deflectors (AOD) (AA-Optoelectronic) were used to form time-shared optical traps with a dwell time of 10 μs from a single CW laser beam. Two orthogonally mounted AODs give independent control of the *x*- and *y*-position of a trap, allowing the formation of 2D arrays of optical traps. The details of the setup are given elsewhere.[14]

Within the parameters defining the optimum optical trap and the hydrogel scaffold, it is still possible to extend the size, shape and constituency of a cell array without compromising viability by using a step-and-repeat methodology.[41] Step-and-repeat involves assembling an array of living cells out of composite voxels, each consisting of a small number of cells that are assembled and encapsulated in hydrogel. Heterogeneous arrays of isogenic voxels of genetically engineered *E. coli* were formed this way. Typically, several regular 2D 3 × 3 or 4 × 4 voxels spaced ∼30 μm apart comprised each array.

All the trapping took place in the center of the microfluidic in near-stagnant flow conditions. Bacteria were captured individually and placed into the time-shared array of optical traps using a freely definable shepherd beam; time-averaged powers in the array and shepherd beam were ∼5 and ∼20 mW respectively. Assembly of a 2D 3 × 3 isogenic voxel required <3 min, typically.

Prepolymer Solution. To minimize exposure to the laser beam, the bacteria were encapsulated in hydrogel.[41] Hydrogel prepolymer solution consisted of 3400 Da polyethylene glycol diacrylate (PEGDA) (Laysan Bio) dissolved in M9 (0.2% glycerol) minimal media to yield 8% (w/v) final concentration and the photoinitiator, 2-hydroxy-2-methyl-propiophenone (Sigma), at a concentration of 0.1−0.2% (w/v). The prepolymer mixture was vortexed for 1 min, and then loaded into 1 mL syringes. Tubing was attached to each syringe *via* a 23-gauge needle; it was then filled and connected to the microfluidic device. The prepolymer solution was photopolymerized using a metal halide light source (X-CITE 120Q, Lumen Dynamics) and a 340 ± 13 nm bandpass UV filter (Semrock). A square mask (∼5.6 mm × 5.6 mm) placed in front of the UV source was used to control the shape and size

DOI: 10.1021/acssynbio.6b00002
ACS Synth. Biol. XXXX, XXX, XXX−XXX

of the hydrogel spot. The light generated by the lamp was focused using a Köhler light train described elsewhere.[41]

Fluorescence Imaging. Immediately after photopolymerization and flushing the array with M9, we began monitoring the fluorescence. The same metal halide light source used for photopolymerization of the hydrogel was also used for fluorescence excitation. The fluorescence from proteins GFP-LVA was captured with a Zeiss Neofluer 40× NA 1.3 objective using a cooled CCD camera (Orca-R2, Hamamatsu) and in combination with a GFP filter set (59022, Chroma) and a single band excitation filter. Time-lapse images were recorded as 16-bit grayscale Tagged Image File Format images (TIFF) using software written in LabView (V8.6, National Instruments).

The fluorescence images were processed using ImageJ (NIH), MATLAB (v7.10.0, Mathworks) and Imaris. The data was read into 2D numerical arrays containing the intensity values of each pixel in the image. The mean of the raw pixel intensity values from each cell in each time-lapse image was extracted using a technique described elsewhere[14] yielding the time-intensity kymographs. This reveals a distribution of response times associated with an ROI—information like this is usually obscured in bulk measurements of the fluorescence that cannot monitor the same cell at different times.

Simulation of the Dynamic Response of Transmitters/Receivers to an Inducer. *Finite Element Simulation.* The stationary Navier−Stokes equation describes flow in the channel, *i.e.*,

$$\rho(v\cdot\nabla v) = -\nabla p + \mu\nabla^2 v$$

where ρ is the density of water, v is the velocity, p is the pressure and η is the viscosity. The time dependent diffusion of the signaling molecule in the channel is given by:

$$\frac{\partial c}{\partial t} + \nabla\cdot cv = D_0\nabla^2 c$$

where c is the concentration. The diffusion coefficient of HSL or inducer in the fluid phase, D_0, is estimated from the Stokes−Einstein equation, $D_0 = k_B T = 6\pi\eta r_s$, where k_B is Boltzmann's constant, T is the temperature and r_s is the mean radius of the molecule. Mass transport in the saturated hydrogel is described by:

$$\varphi\frac{\partial c}{\partial t} + \nabla\cdot cv = D_g\nabla^2 c + S$$

where φ represents the porosity of the hydrogel and S is a source term accounting for the production of signal by the transmitters. Diffusion in the gel, D_g, is given by:

$$\frac{D_g}{D_0} = \left(\frac{1-\varphi}{1+\varphi}\right)^2$$

The flow and the diffusion/convection of the signaling molecules was simulated using COMSOL Multiphysics (v4.2).

Simulation of Dynamic Gene Expression. The complex processes associated with protein production, *i.e.*, gene transcription and mRNA translation, were assembled into a model (Figure S3a,b) that was based, in part, on the deterministic equations described by Goryachev *et al.*[31] and Stamatakis and Mantzaris.[32] Briefly, for the *lux/lac* model, the inducer, IPTG, which can freely diffuse into and out of the cell through the membrane, binds to lacI and promotes production of luxI-LVA and GFP-LVA. LuxI-LVA produces $3OC_6HSL$, which in turn can diffuse out through the cell membrane. Likewise for the *las/arab* model, the inducer, arabinose, which can freely diffuse into and out of the cell through the membrane, binds to lasI and promotes production of lasI-lva and GFP-LVA. LasI-LVA produces $3OC_{12}HSL$, which slowly diffuses out through the cell membrane.

Deterministic models based on mass action equations were developed in order to describe the genetic processes leading to the production of LuxI, $3OC_6HSL$, LuxR, LasI, $3OC_{12}HSL$, LasR and GFP in each cell (Figure S3a,b). The rate equations and parameters for these models (eqs S(i−xxiv) and S(xxv−li) for the *lux*- and *las*-comlinks, respectively) were based on equations described elsewhere,[14] and implemented and solved using MATLAB (The MathWorks, ver. 2015b, Natick, MA). Starting with the values compiled from the literature,[31,32] a nonlinear least-squares algorithm was used to find the variables that best matched the fluorescence data, constrained by the uncertainties specified in Tables S1−S6. Variability associated with the uncertainty in the rates introduced a stochastic element into the processes. These models provided a means to track the dynamics of each species in response to variations in the external HSL concentration. The number of species in each cell are calculated from macroscopic quantities by taking into account the estimated volume of the cell: 1 molecule per cell corresponds to approximately $1/(V\cdot N_A) = 1.7$ nM, where N_A is Avogadro's number. For each simulation, external HSL (A_{ex}) was treated as a boundary condition and was not varied by the simulation, but depended on the flow condition imposed on the cells in the experiment.

■ ASSOCIATED CONTENT

Supporting Information

The Supporting Information is available free of charge on the ACS Publications website at DOI: 10.1021/acssynbio.6b00002.

Supporting equations, tables, and figures (PDF)

■ AUTHOR INFORMATION

Corresponding Author

*E-mail: gtimp@nd.edu.

Author Contributions

†NP and EMN contributed equally to this work.

Notes

The authors declare no competing financial interest.

■ ACKNOWLEDGMENTS

This work was supported by NSF CCF-1129098 and the Keough-Hesburgh chair. We gratefully acknowledge the assistance of V. Kurz with optics and K. Sarveswaran with LCL.

■ REFERENCES

(1) Simpson, M. L., Sayler, G. S., Fleming, J. T., and Applegate, B. (2001) Whole-cell biocomputing. *Trends Biotechnol. 19* (8), 317−321.

(2) Hasty, J., McMillen, D., and Collins, J. J. (2002) Engineered gene circuits. *Nature 420*, 224−230.

(3) Weiss, R., Basu, S., Hooshangi, S., Kalmbach, A., Karig, D., Mehreja, R., and Netravli, I. (2003) Genetic circuit building blocks for cellular computation, communications, and signal processing. *Nat. Comput. 2*, 47−84.

(4) Ellis, T., Wang, X., and Collins, J. J. (2009) Diversity-based, model-guided construction of synthetic gene networks with predicted functions. *Nat. Biotechnol. 27* (5), 465−471.

DOI: 10.1021/acssynbio.6b00002
ACS Synth. Biol. XXXX, XXX, XXX−XXX

(5) Wang, B., Kitney, R., Joly, N., and Buck, M. (2011) Engineering modular orthogonal genetic logic gates for robust digital-like synthetic biology. *Nat. Commun. 2*, 508.
(6) Siuti, P., Yazbek, J., and Lu, T. K. (2013) Synthetic circuits integrating logic and memory in living cells. *Nat. Biotechnol. 31*, 448.
(7) Gardner, T. S., Cantor, C. R., and Collins, J. J. (2000) Construction of a genetic toggle switch in Escherichia coli. *Nature 403*, 339−342.
(8) Tamsir, A., Tabor, J. J., and Voigt, C. A. (2011) Robust multicellular computing using genetically encoded NOR gates and chemical 'wires'. *Nature 469*, 212−215.
(9) Guet, C., Elowitz, M., Hsing, W., and Leibler, S. (2002) Combinatorial synthesis of genetic networks. *Science 296*, 1466−1470.
(10) Anderson, J. C., Voigt, C. A., and Arkin, A. P. (2007) Environmental signal integration by a modular AND gate. *Mol. Syst. Biol. 3*, 133.
(11) Moon, T. S., Lou, C., Tamsir, A., Stanton, B. C., and Voigt, C. A. (2012) Genetic programs constructed from layered logic gates in single cells. *Nature 491*, 249−253.
(12) Bonnet, J., Yin, P., Ortiz, M. E., Subsoontorn, P., and Endy, D. (2013) Amplifying Genetic Logic Gates. *Science 340*, 599.
(13) Danino, T., Mondragón-Palomino, O., Tsimring, L., and Hasty, J. (2010) A synchronized quorum of genetic clocks. *Nature 463*, 326−330.
(14) Nelson, E. M., Kurz, V., Perry, N., and Timp, G. (2013) Biological Noise Abatement: Coordinating the Responses of Autonomous Bacteria in a Synthetic Biofilm to a Fluctuating Environment Using a Stochastic Bistable Switch. *ACS Synth. Biol. 3*, 286.
(15) Zhou, T., Chen, L., and Aihara, K. (2005) Molecular Communication through Stochastic Synchronization Induced by Extracellular Fluctuations. *Phys. Rev. Lett. 95*, 178103.
(16) Ullner, E., Zaikin, A., Volkov, E. I., and Garica-Ojalvo, J. (2007) Multistability and Clustering in a Population of Synthetic Genetic Oscillators via Phase-Repulsive Cell-to-Cell Communications. *Phys. Rev. Lett. 99*, 148103.
(17) Chen, Y., Kyoung Kim, J., Hirning, A. J., Josić, K., and Bennet, M. R. (2015) Emergent genetic oscillations in a synthetic microbial consortium. *Science 349*, 986−989.
(18) Basu, S., Gerchman, Y., Collins, C. H., Arnold, F. H., and Weiss, R. (2005) A synthetic multicellular system for programmed pattern formation. *Nature 434*, 1130−1134.
(19) You, L., Cox, R. S., Weiss, R., and Arnold, F. H. (2004) Programmed population control by cell−cell communication and regulated killing. *Nature 428*, 868−871.
(20) Brenner, K., Karig, D. K., Weiss, R., and Arnold, F. H. (2007) Engineered bidirectional communication mediates a consensus in a microbial biofilm consortium. *Proc. Natl. Acad. Sci. U. S. A. 104* (44), 17300−17304.
(21) Nadell, C. D., Bassler, B. L., and Levin, S. A. (2008) Observing bacteria through the lens of social evolution. *J. Biol. 7*, 27.
(22) Nadell, C. D., Xavier, J. B., Levin, S. A., and Foster, K. R. (2008) The Evolution of Quorum Sensing in Bacterial Biofilms. *PLoS Biol. 6* (1), e14.
(23) Dufour, D., Leung, V., and Lévesque, C. M. (2010) Bacterial biofilm: structure, function, and antimicrobial resistance. *Endodontic Topics 22*, 2−16.
(24) Fuqua, C., Parsek, M. R., and Greenberg, E. P. (2001) Regulation of gene expression by cell-to-cell communication: acyl-homoserine lactone quorum sensing. *Annu. Rev. Genet. 35*, 439−468.
(25) Miller, M. B., and Bassler, B. L. (2001) Quorum sensing in bacteria. *Annu. Rev. Microbiol. 55*, 165−169.
(26) Weiss, R., and Knight, T. (2001) Engineered communications for microbial robotics. In *DNA Computing*, pp 1−16, Springer, Berlin.
(27) Nealson, K., Platt, T., and Hastings, J. W. (1970) The cellular control of the synthesis and activity of the bacterial luminescent system. *J. Bacteriol. 104*, 313−22.
(28) Sauer, K., Camper, A., Ehrlich, G., Costerton, J., and Davies, D. (2002) *Pseudomonas aeruginosa* displays multiple phenotypes during development as a biofilm,". *J. Bacteriol. 184*, 1140−54.
(29) Timp, W., Mirsaidov, U., Matsudaira, P., and Timp, G. (2009) Jamming Prokaryotic Cell-to-Cell Communications in a Model Biofilm. *Lab Chip 9* (7), 925−934.
(30) Kurz, V., Nelson, E., Perry, N., Timp, W., and Timp, G. (2013) Epigenetic Memory Emerging from Integrated Transcription Bursts. *Biophys. J. 105*, 1526−32.
(31) Goryachev, A. B., Toh, D. J., and Lee, T. (2006) Systems analysis of a quorum sensing network: Design constraints imposed by the functional requirements, network topology and kinetic constants. *BioSystems 83*, 178−187.
(32) Stamatakis, M., and Mantzaris, N. V. (2009) Comparison of Deterministic and Stochastic Models of the lac Operon Genetic Network,. *Biophys. J. 96*, 887−906.
(33) Wargo, M. J., and Hogan, D. A. (2007) Examination of *Pseudomonas aeruginosa* lasI regulation and 3-oxo-C12-homoserine lactone production using a heterologous Escherichia coli system. *FEMS Microbiol. Lett. 273*, 38−44.
(34) Smith, R. S., Kelly, R., Iglewski, B. H., and Phipps, R. P. (2002) The *Pseudomonas* autoinducer N-(3-oxododecanoyl) homoserine lactone induces cyclooxygenase-2 and prostaglandin E2 production in human lung fibroblasts: implications for inflammation. *J. Immunol. 169*, 2636−2642.
(35) Winson, M. K., Swift, S., Fish, L., Throup, J. P., Örgensen, F. J., Chhabra, S. R., Bycroft, B. W., Williams, P., and Stewart, G. S. A. B. (1998) Construction and analysis of luxCDABE-based plasmid sensors for investigating N-acyl homoserine lactone-mediated quorum sensing. *FEMS Microbiol. Lett. 163*, 185−192.
(36) Gray, K. M., Passador, L., Iglewski, B. H., and Greenberg, E. P. (1994) Interchangeability and Specificity of Components from the Quorum-sensing Regulatory Systems of *Vibrio Fischeri* and *Pseudomonas aeruginosa*. *J. Bacteriol. 176*, 3076−3080.
(37) Schuster, M., Urbanowski, M. L., and Greenberg, E. P. (2004) Promoter specificity in *Pseudomonas aeruginosa* quorum sensing revealed by DNA binding of purified LasR. *Proc. Natl. Acad. Sci. U. S. A. 101*, 15833−15839.
(38) Urbanowski, M. L., Lostroh, C. P., and Greenberg, E. P. (2004) Reversible Acyl-Homoserine Lactone Binding to Purified *Vibrio fischeri* LuxR Protein. *J. Bacteriol. 186*, 631−637.
(39) Karig, D. K., Siuti, P., Dar, R. D., Retterer, S. T., Doktycz, M. J., and Simpson, M. L. (2011) Model for biological computation in a nanfabricated cell-mimic driven by stochastic resonance. *Nano. Commun. Netw. 2*, 39−49.
(40) Pérez, P. D., Weiss, J. T., and Hagen, S. J. (2011) Noise and crosstalk in two quorum-sensing inputs of Vibrio fischeri. *BMC Syst. Biol. 5*, 153.
(41) Mirsaidov, U., Scrimgeour, J., Timp, W., Beck, K., Mir, M., Matsudaira, P., and Timp, G. (2008) Live Cell Lithography: Using Optical Tweezers to Create Synthetic Tissue. *Lab Chip 8*, 2174−2181.
(42) Williams, W., Cui, W., Levchenko, A., and Stevens, A. M. (2008) Robust and sensitive control of a quorum-sensing circuit by two interlocked feedback loops. *Mol. Syst. Biol. 4*, 234.
(43) Andersen, J. B., Sternberg, C., Poulsen, L., Bjorn, S., Givskov, M., and Molin, S. (1998) New unstable variants of green fluorescent protein for studies of transient gene expression in bacteria. *Appl. Environ. Microbiol. 64*, 2240.
(44) Balasubramanian, D., Schneper, L., Kumari, H., and Mathee, K. (2013) A dynamic and intricate regulatory network determines *Pseudomonas aeruginosa* virulence. *Nucleic Acids Res. 41*, 1−20.
(45) Redfield, R. (2002) Is quorum sensing a side effect of diffusion sensing? *Trends Microbiol. 10*, 365−370.
(46) Hense, B. A., Kuttler, C., Müller, J., Rothballer, M., Hartmann, A., and Kreft, J.-U. (2007) Does efficiency sensing unify diffusion and quorum sensing? *Nat. Rev. Microbiol. 5*, 230−239.
(47) Horswill, A. R., Stoodley, P., Stewart, P. S., and Parsek, M. R. (2007) The effect of the chemical, biological, and physical environ-

DOI: 10.1021/acssynbio.6b00002
ACS Synth. Biol. XXXX, XXX, XXX−XXX

ment on quorum sensing in structured microbial communities. *Anal. Bioanal. Chem. 387*, 371−380.
(48) Schuster, M., Lostroh, C. P., Ogi, T., and Greenberg, E. P. (2003) Identification, Timing, and Signal Specificity of *Pseudomonas aeruginosa* Quorum-Controlled Genes: a Transcriptome Analysis. *J. Bacteriol. 185*, 2066−2079.
(49) Pearson, J. P., Van Delden, C., and Iglewski, B. H. (1999) Active efflux and diffusion are involved in transport of Pseudomonas aeruginosa cell-to-cell signals. *J. Bacteriol. 181* (4), 1203−10.
(50) Krol, E., and Becker, A. (2014) Rhizobial homologs of the fatty acid transporter FadL facilitate perception of long-chain acyl-homoserine lactone signals. *Proc. Natl. Acad. Sci. U. S. A. 111*, 10702−7.
(51) Typas, A., and Sourjik, V. (2005) Bacterial protein networks: properties and function. *Nat. Rev. Microbiol. 13*, 559.
(52) Mead, C. (1989) *Analog VLSI and Neural Systems*, pp 155−158, Addison-Wesley, New York.
(53) Booth, T. L. (1971) *Digital Networks and Computer Systems*, pp 1−256, John Wiley and Sons, Inc., New York.
(54) Suzuki, M., Mao, L., and Inouye, M. (2007) Single protein production (SPP) system in Escherichia coli. *Nat. Protoc. 2*, 1802−1810.
(55) Nelson, E. M., Mirsaidov, U., Sarveswaran, K., Perry, N., Kurz, V., Timp, W., and Timp, G. (2015) Ecology of a Simple Synthetic Biofilm. In *The Physical Basis of Bacterial Quorum Communication* (Hagen, S., Ed.) pp 205−226, Springer, New York.
(56) Win, M. N., and Smolke, C. D. (2008) Higher-Order Cellular Information Processing with Synthetic RNA Devices,. *Science 322*, 456−460.
(57) Liu, W.-T., private communication.
(58) Torvinen, E., Lehtola, M. J., Martikainen, P. J., and Miettinen, I. T. (2007) Survival of Mycobacterium avium in drinking water biofilms as affected by water flow velocity, availability of phosphorus, and temperature. *Appl. Environ. Microbiol. 73*, 6201−6207.
(59) Lehtola, M. J., Torvinen, E., Kusnetsov, J., Pitkänen, T., Maunula, L., Bonsdorff, C. H., Wilks, S. A., Keevil, C. W., and Miettinen, I. T. (2007) Survival of Mycobacterium avium, Legionella pneumophila, Escherichia coli, and caliciviruses in drinking water-associated biofilms grown under high-shear turbulent flow. *Appl. Environ. Microbiol. 73*, 2854−9.
(60) Storey, M. V., Langmark, J., Ashbolt, N. J., and Stenstrom, T. A. (2004) The fate of legionellae within distribution pipe biofilms: measurement of their persistence, inactivation and detachment. *Water Sci. Technol. 49*, 269−275.

DOI: 10.1021/acssynbio.6b00002
ACS Synth. Biol. XXXX, XXX, XXX−XXX